International Journal of Heat and Fluid Flow 30 (2009) 729–740

Contents lists available at ScienceDirect

International Journal of Heat and Fluid Flow

journal homepage: www.elsevier.com/locate/ijhff

Heat and mass transfer of a fuel droplet evaporating in oscillatory flow

M. Jangi *, H. Kobayashi

Institute of Fluid Science, Tohoku University, 2-1-1 Katahira, Aoba-ku, Sendai, Miyagi 980-8577, Japan

ARTICLE INFO

Article history:
Received 4 June 2008
Received in revised form 23 March 2009
Accepted 24 March 2009
Available online 28 April 2009

Keywords:
Droplet evaporation
Unsteady boundary layer
Oscillatory flow

ABSTRACT

A numerical study of the heat and mass transfer from an evaporating fuel droplet in oscillatory flow was performed. The flow was assumed to be laminar and axisymmetric, and the droplet was assumed to maintain its spherical shape during its lifetime. Based on these assumptions, the conservation equations in a general curvilinear coordinate were solved numerically. The behaviors of droplet evaporation in the oscillatory flow were investigated by analyzing the effects of flow oscillation on the evaporation process of a *n*-heptane fuel droplet at high pressure.

The response of the time history of the square of droplet diameter and space-averaged Nusselt numbers to the main flow oscillation were investigated in frequency band of 1–75 Hz with various oscillation amplitudes. Results showed that, depending on the frequency and amplitude of the oscillation, there are different modes of response of the evaporation process to the flow oscillation. One response mode is synchronous with the main flow oscillation, and thus the quasi-steady condition is attained. Another mode is asynchronous with the flow oscillation and is highly unsteady. As for the evaporation rate, however, in all conditions is more greatly enhanced in oscillatory flow than in quiescent air.

To quantify the conditions of the transition from quasi-steady to unsteady, the response of the boundary layer around the droplet surface to the flow oscillation was investigated. The results led to including the oscillation Strouhal number as a criteria for the transition. The numerical results showed that at a low Strouhal number, a quasi-steady boundary layer is formed in response to the flow oscillation, whereas by increasing the oscillation Strouhal number, the phenomena become unsteady.

1. Introduction

Heat and mass transfer from a sphere in oscillatory flow has been investigated since 1930 (Marthelli and Boelter, 1938). These phenomena are interesting because of their application in practical spray evaporation and combustion in the presence of oscillatory waves (Sabnis and Lyman, 1982; Masahiro et al., 1996; Tanabea et al., 2005) and drying (Lockwood, 1980). Analytical and numerical simulations of the flow oscillation effects on the rate of heat and mass transfer from a sphere have been performed to investigate the mechanism of the enhancement of the transport phenomena due to flow oscillation. Burdukov and Nakoryakov (1965), Riley (1966), Strahle (1965) have investigated these phenomena using the perturbation method. However, this method is limited to cases in which the displacement of an element of mass in the free stream is much less than the sphere diameter. The development of computers and numerical methods has enabled the numerical investigation of these phenomena over a wide range of conditions. Drummound (1990) has simulated the mass transfer from a sphere in an oscillating flow using the pseudo spectral method and has studied the phenomena with Re_a of 1–150 Hz and Strouhal number of 1–1000. Ha and Yavuzkurt (1993) have numerically investigated the mechanism of the enhancement of the heat and mass transfer from a sphere in acoustic oscillating flow. They have shown that oscillation in the range of Re_a of 10–100 with a frequency of 50–2000 Hz can enhance the rate of transport phenomena up to 290% compared with those in quiescent air.

Recently, it has been shown experimentally that turbulence can affect the evaporation rate of a single droplet (Gökalp et al., 1992; Hiromitsu and Kawaguchi, 1995; Birouk and Gökalp, 2002, 2006; Wu et al., 2001, 2003; Abou AlSood and Birouk, 2007, 2008). It is known that a turbulent flow field consists of many vortex tubes over a wide range of length and time scales (Vincent and Meneguzzi, 1991; Gotoh et al., 2002). Masoudi and Sirignano (2000) have studied numerically the interaction between a vortex and an evaporating droplet. Their three-dimensional simulation of the collision of a vortex with a vaporizing droplet led to proposing an equation for modifying the averaged Nusselt number (Nu_{av}) and Sherwood number (Sh_{av}) of an axisymmetric system, for the case of vortex–droplet collision. While the studies on the vortex–droplet system performed by Gökalp et al. (1992), Hiromitsu and Kawaguchi (1995), Birouk and Gökalp (2002), Wu et al. (2001, 2003), Birouk and Gökalp (2006), Abou AlSood and Birouk (2007, 2008), Masoudi and Sirignano (2000) have focused on the cases in which

* Corresponding author. Present address: Department of Flow, Heat and Combustion Mechanics, Gent University, Belgium.
E-mail address: mehdi.jangi@ugent.be (M. Jangi).

0142-727X/$ - see front matter © 2009 Elsevier Inc. All rights reserved.
doi:10.1016/j.ijheatfluidflow.2009.03.012

Nomenclature

δt	time step
λ	thermal conductivity
μ	viscosity
ϕ	variable
ρ	density
v	velocity vector
τ	$1 - T_r$
C_p	specific heat at constant pressure
C_v	specific heat at constant volume
d	droplet diameter
D_{im}	mixture mass diffusivity of ith species
f	oscillation frequency
h_i	enthalpy of ith species
H_{fg}	latent heat of vaporization
M	fuel molecular weight
n	direction normal to the droplet surface
N_{u_θ}	local Nusselt number
$N_{u_{av}}$	space averaged Nusselt number
p	pressure
P_c	fuel critical pressure
P_v	fuel vapor partial pressure
P_{vpr}	reduced vapor pressure P_v/P_c
R	droplet radius
r	radial coordinate
Re_∞	droplet/sphere Reynolds number $\rho_\infty U_\infty d_0/\mu_\infty$
Re_a	oscillation Reynolds number $\rho_\infty U_a d_0/\mu_\infty$
Res_ϕ	residual of ϕ variable
S_{osc}	oscillation Strouhal number
Sh_θ	local Sherwood number
Sh_{av}	space averaged Sherwood number
T	temperature
t	time
T_c	fuel critical temperature
T_r	reduced temperature T/T_c
U	axial component of velocity
U_a	oscillation velocity amplitude
V	radial component of velocity
v_θ	tangential velocity at interface
V_i	diffusion velocity of ith species
v_n	velocity normal to interface
X	mole fraction
x	axial coordinate
Y_i	mass fraction of ith species

Subscripts

∞	free stream
av	space averaged
f	fuel
g	gas phase
i	ith species
l	liquid phase
s	droplet interface
+	interface in gas phase side
−	interface in liquid phase side
0	initial condition

vortex diameters are smaller than the droplets (see Fig. 1b), Mitsuya et al. (2005) have proposed another model of droplet–vortex interaction considering the turbulence structure and have shown that in a practical spray combustor, a significant portion of the droplet–vortex interaction takes place in the region where the vortex diameter is larger than droplet size as shown in Fig. 1a. According to Mitsuya et al. (2005), it is expected that the interaction between the vortex tubes and droplet motion in a fuel spray produces an oscillatory relative velocity between the droplet and main flow (Mitsuya et al., 2005). Since the dimension of droplets in practical sprays are much smaller (e.g. 50 μm) than what is required for a droplet combustion experiment in microgravity (e.g. 1 mm), it is necessary to render the phenomena in a much larger system, so that the dimension of the droplet is large enough for performing such experiments. Mistuya et al. then rescaled the system of droplet–vortex through introducing three non-dimensional parameters of droplet time, initial Reynolds number and oscillatory Reynolds number (Mitsuya et al., 2005). They have shown that the flow frequency needed to simulate turbulent motion of the droplet is on the order of 10 Hz if the oscillation Reynolds number is between 10 and 100 (Mitsuya et al., 2005) and droplet diameter is about 1 mm. The purpose of the present numerical study is to understand the characteristics and mechanism of the evaporation of a fuel droplet in the presence of flow oscillation with a frequency range of 1–75 Hz and oscillation Reynolds number from 1 to 100 consistent with the microgravity experiments that have been performed previously (Mitsuya et al., 2005; Ogami et al., 2009; Jangi et al., in press) based on the Mitsuya et al. model (Mitsuya et al., 2005).

2. Mathematical model

A schematic of the model under study is shown in Fig. 2. The center of the droplet is fixed in space and oscillatory air flows around it. Since the relative velocity between droplets and the main flow is very small in practical combustors (Faeth, 1983), we are interested in investigating oscillatory flow, with the maximum droplet Reynolds number Re_a below 100. This range is also consistent with the analysis by Mitsuya et al. (2005). In such a small Re_a, flow is laminar and axisymmetric (Clift et al., 1978; Bagchi et al., 2001). For the liquid phase, it was assumed that the droplet maintains a spherical shape. To include transient heating up of the droplet and flow circulation inside a droplet with time and space variables thermo-physical properties of the liquid phase were considered (Appendix A). The transport properties for the gas phase vary with time and space and are evaluated by linking the CHEMKIN package to the code. Based on the above-mentioned assumptions, the governing equations in the gas phase, liquid phase and at the interface between the gas and liquid are as follows:

Continuity:

$$\frac{\partial \rho}{\partial t} + \nabla \cdot (\rho \mathbf{v}) = 0, \tag{1}$$

momentum conservation:

$$\rho \frac{\partial \mathbf{v}}{\partial t} + \rho \mathbf{v} \cdot \nabla \mathbf{v} = -\nabla \mathrm{p} - \nabla \left[\frac{2}{3} \mu (\nabla \cdot \mathbf{v}) \right] + \nabla \cdot \left\{ \mu \left[(\nabla \mathbf{v}) + (\nabla \mathbf{v})^{\mathrm{T}} \right] \right\}, \tag{2}$$

energy conservation:

$$\frac{\partial}{\partial t}(\rho C_v T) + \nabla \cdot (\rho C_p \mathbf{v} T) = \nabla \cdot (\lambda \nabla T) - \sum \rho Y_i \mathrm{V}_i \cdot \nabla h_i, \tag{3}$$

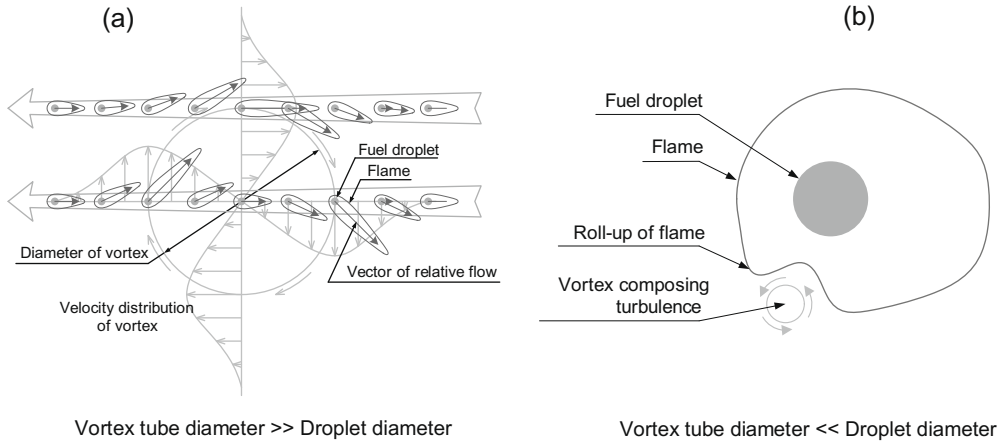

Fig. 1. Schematic illustration of the Mitsuya model of droplet–vortex interaction ((b) after Mitsuya et al. (2005)).

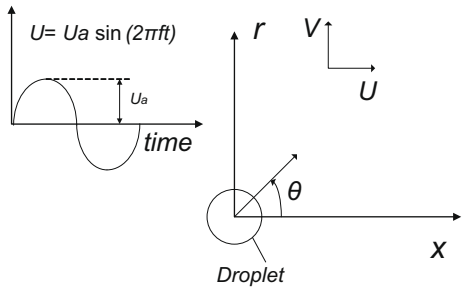

Fig. 2. Schematic of single droplet in oscillatory flow.

conservation of species:

$$\frac{\partial}{\partial t}(\rho Y_i) + \nabla \cdot (\rho \mathbf{v} Y_i) = \nabla \cdot (\rho D_{im} \nabla Y_i). \tag{4}$$

In this study, the diffusion velocity V_i is defined as

$$V_i = (-D_{im}/Y_i)\nabla Y_i. \tag{5}$$

At the interface between gas and liquid, the following equations are employed.

Conservation of mass:

$$\rho_+\left(v_{n+} - \frac{dR}{dt}\right) = \rho_-\left(v_{n-} - \frac{dR}{dt}\right), \tag{6}$$

conservation of species:

$$\rho_+ Y_{i+}\left(v_{n+} + V_{i+} - \frac{dR}{dt}\right) = \rho_- Y_{i-}\left(v_{n-} + V_{i-} - \frac{dR}{dt}\right), \tag{7}$$

conservation of energy:

$$\lambda_+\left(\frac{\partial T}{\partial n}\right)_+ = \lambda_-\left(\frac{\partial T}{\partial n}\right)_- + \rho_+ H_{fg}\left(v_{n+} - \frac{dR}{dt}\right), \tag{8}$$

continuity of tangential velocity:

$$v_{\theta+} = v_{\theta-}. \tag{9}$$

Assuming that the gas and liquid phases are in local dynamic equilibrium, the mole fraction X_{f+} of the fuel component in the gas phase can be calculated according to $X_{f+} = P_v/P$. The vapor pressure is computed based on an extension of the Calusius–Clapeyron equation (Poling et al., 2000; Ambrose and Ghiassee, 1987):

$$\ln P_{vpr} = (C_1\tau + C_2\tau^{1.5} + C_3\tau^{2.5} + C_4\tau^5)/T_r \tag{10}$$

where P_c and T_c are the critical pressure and temperature, respectively, P_{vpr} is $P_v/P_c, T_r$ is $T/T_c, \tau$ is $1 - T_r$ and C_1, C_2, C_3 and C_4 are constants for a given fuel (Poling et al., 2000). The mass fraction of the fuel vapor Y_f is then given by

$$Y_f = \frac{M_f X_f}{\sum M_i X_i}. \tag{11}$$

Since we consider a single component droplet, the evaporation rate $\dot{m}_v''$ can be described according to Eq. (7) for $i = f$:

$$\dot{m}_v'' = \dot{m}_v'' Y_{f+} + \rho_+ Y_{f+} V_{f+}. \tag{12}$$

To obtain the solution even for $Y_{f+} = 1$, an alternative equation for Eq. (12) based on energy conservation Eq. (8) is needed as:

$$\dot{m}_v'' = \frac{1}{H_{fg}}\left[\lambda_+\left(\frac{\partial T}{\partial n}\right)_+ - \lambda_-\left(\frac{\partial T}{\partial n}\right)_-\right]. \tag{13}$$

The surface regression rate dR/dt is then calculated by integrating $\dot{m}_v''$ at the interface as below:

$$\frac{dR}{dt} = -\left(\frac{1}{4\pi R^2 \rho_l}\right)\oint \dot{m}_v'' dA + \frac{R}{3\rho_l}\frac{d\rho_l}{dt}. \tag{14}$$

According to Fig. 2, the governing equations (1)–(4) have the following boundary conditions:at $r = 0$, symmetry conditions

$$\frac{\partial \rho}{\partial r} = 0, \quad \frac{\partial u}{\partial r} = 0, \quad \frac{\partial T}{\partial r} = 0, \quad \frac{\partial(\rho Y_i)}{\partial r} = 0, \quad v = 0. \tag{15}$$

and at $r \to \infty$,

$$\begin{aligned} &U = U_a \cos(2\pi f t), \\ &V = 0, \\ &T = T_\infty, \quad Y_i = Y_{i\infty}, \quad p = p_\infty. \end{aligned} \tag{16}$$

At the interface of liquid and gas phases ($r = R$), the boundary conditions have been described in Eqs. (6)–(13). The infinity boundary conditions are assumed to be located at a distance of ten times the initial diameter. Ha and Yavuzkurt assumed the same position of the infinity boundary for the simulation of heat and mass transfer from a sphere in the same oscillatory flows as those analyzed in the present study (Ha and Yavuzkurt, 1993). They used 30 grids along the droplet surface and 50 grids in a radial direction. For confirmation of the location of the infinity boundary condition

and the minimum number of required grids, calculations at $p_\infty = 0.5$ MPa and $T_\infty = 749$ K for the $f = 15$ Hz and $Re_a = 60$ were performed with various domain sizes from 5 to 25 times the initial diameter and with a different number of grids. It was confirmed that the responses of the instantaneous Nu_θ and Nu_{av} and the time history of the square of the droplet diameter are independent of the grids and of the location of the infinity boundary condition when an appropriate number of grids for a domain of larger than 16 times the initial droplet diameter (i.e., more than 80 in a radial direction and 60 along the droplet surface for a domain that is 20 times the initial size of the droplet diameter) were used. This implies that the distance of the infinity boundary condition is 8 times the initial droplet diameter in oscillatory flows.

3. Numerical algorithm

The governing equations were solved numerically using the finite volume method. The power-law scheme was used for convection–diffusion modeling and the SIMPLE (Patankar, 1980) algorithm was applied to solve the flow field. The generalized curvilinear coordinate was adapted to the physical problem. The structured boundary-fitted grids (Farrashkhalvat and Miles, 2003) were generated using Thomas' algorithm and the equations were discretized in spatial collocated boundary-fitted grids. The discretization equations were solved using the alternating direction implicit method with the TDMA used on each line of the two alternating directions. The computational grids toward the droplet surface were concentrated using hyperbolic tangent stretching functions (Vinokur, 1983). The numerical time step was chosen as

$$\delta t = min\left(0.001s, \frac{1}{50f}\right) \tag{17}$$

Sixty grids along the droplet surface and 80 grids in a radial direction in the gas phase and 20 grids in a radial direction in liquid phase were proven to be sufficient to obtain grid independent numerical results in an oscillatory flow. For simulation in the quiescent atmosphere conditions at 0.5 MPa, the number of grids along the droplet surface and in the radial direction was 80×120. Iteration at each time step was performed to achieve the converged solution. The convergence during the iterative procedure was checked by evaluating the imbalance in governing equations (1)–(4). Thus, for variable ϕ, residual Res_ϕ was defined as

$$Res_\phi = \left(\sum_{all\ nodes} \left(a_p \phi_p - \sum_{nb} a_{nb} \phi_{nb} - S_\phi \right)^2 \right)^{0.5}, \tag{18}$$

the global convergence was defined as $Res_\phi < 10^{-6}$ for the all variables. The calculations were continued until the droplet diameter became less than 1/15 of its initial diameter. The validity of code for solving the governing equations was first examined by comparison of the numerical results with available numerical and experimental data in the literature for flow over a sphere for $Re_\infty < 300$.Re_∞ droplet/sphere Reynolds number $\rho_\infty U_\infty d_0/\mu_\infty$ Drag coefficient, reattachment length, separation angle, Nusselt number and Sherwood number were used to compare the numerical results calculated by our code and data in the literature (Clift et al., 1978; Frössling, 1938; Bagchi et al., 2001; Johnson and Patel, 1999). Fig. 3 shows the calculated average Nusslet number Nu_{av} and separation angle θ_s at various Reynolds numbers, and compares those values with the experimental data available in Frössling (1938), Clift et al. (1978). The numerical results using our code were in very good agreement with all of the tested cases. In the next section, the validity of the code for calculation of the evaporating droplet is shown first, and then the behavior of the evaporating droplet in oscillatory flow is investigated by measuring the response of heat and mass transfer to and from a single *n*-heptane droplet in the oscillatory flow.

4. Results and discussion

4.1. Evaporating droplet in steady main flow

In order to check the validity of the numerical calculation, we compared the results of the present simulation with the experimental data reported by Nomura et al. (1996) and the numerical analysis performed by Zhang (2004) for a vaporizing *n*-heptane fuel droplet. Also comparison with the experimental data of Wong and Lin (1992) for a *n*-decane fuel droplet and numerical analysis performed by Abou AlSood and Birouk (2007), Megaridis (1993) were made. These comparisons were performed for the time history of the square of droplet diameter for evaporation of an *n*-hep-

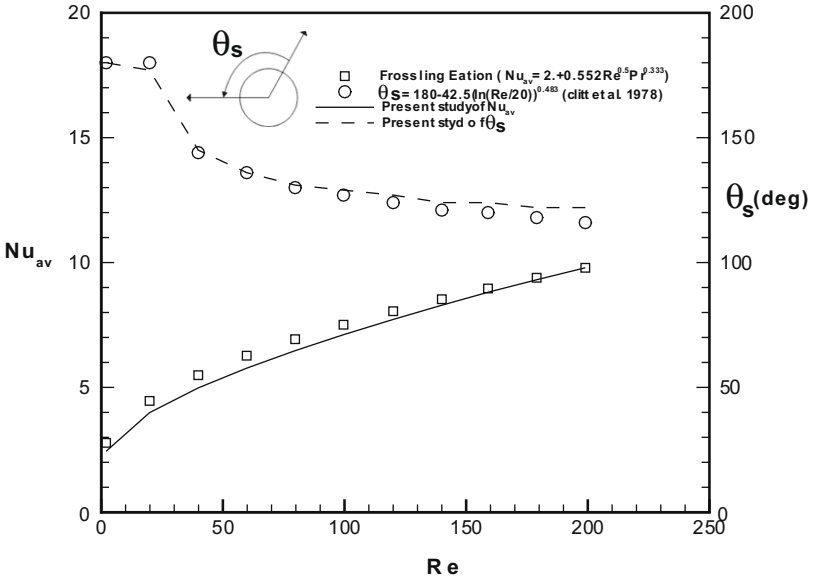

Fig. 3. Comparison of the present numerical results with the experimental data of flow over a sphere.

tane droplet in a quiescent hot atmosphere of $T_\infty = 741$ K and *n*-decane at $Re_\infty = 17$ and hot airstream of temperature $T_\infty = 1000$ K. To simulate the quiescent atmosphere in numerical code, a very small far-flow velocity $U_\infty = 10^{-5}$ m/s was used. Fig. 4a shows the time history of the square of droplet diameter at 0.1 MPa. Although Nomura et al. attempted to provide data of the droplet evaporation in quiescent air, in their experiment the droplet was moved from the droplet generator to the test position in 0.16 s at the beginning of the experiment (Nomura et al., 1996). The effect was reported by Zhang (2004) as well. Comparison of our numerical results with those of Zhang shows the excellent agreement. Fig. 4b shows the time history of the square of droplet diameter at 0.1 MPa and $Re_\infty = 17 = 741$ K. The deviation between our results and those of Wong and Lin (1992) were due to radiation effects at high temperature. Specifically the initial size of droplet $d_0 = 1.961$ mm $= 741$ K in this case was quite large and the radiative heat transfer during the transient heating up of the droplet

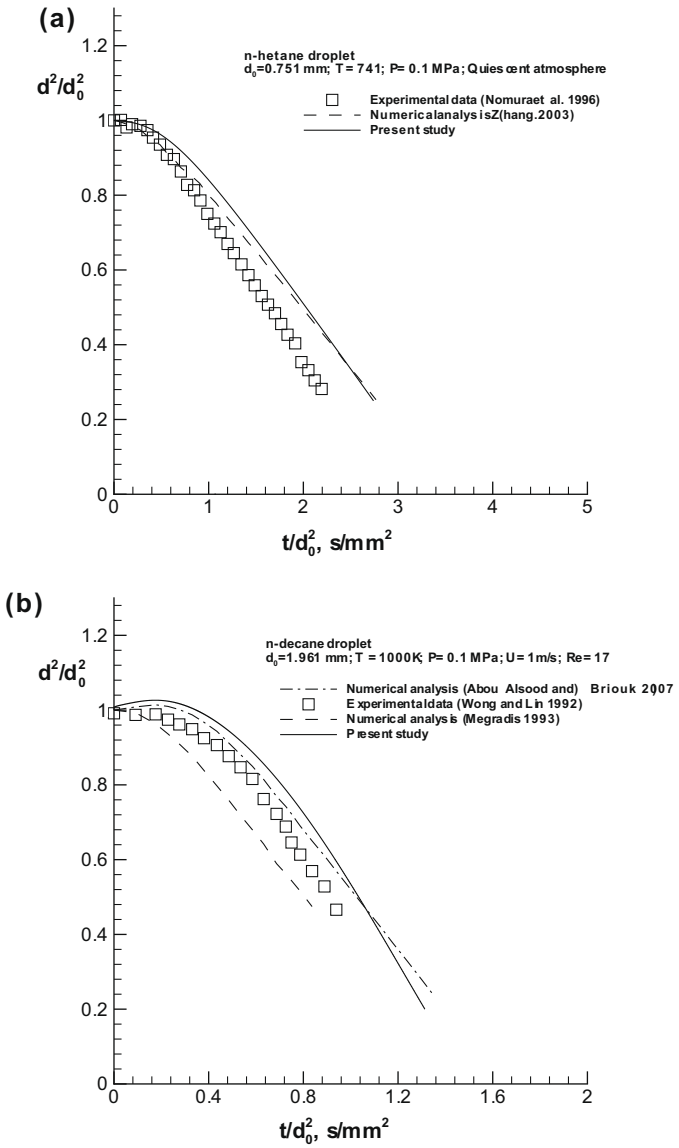

Fig. 4. Comparison of the present numerical results with experimental data of an evaporating droplet: (a) *n*-heptane at ambient pressure 0.1 MPa and ambient temperature 741 K for $d_0 = 0.751$ mm in quiescent air; (b) *n*-decane at ambient pressure 0.1 MPa and ambient temperature 1000 K for $d_0 = 1.961$ mm and $Re_\infty = 17$.

plays an important role (Marchese and Dryer, 1997). A small deviation between our results and those of Abou Alsood and Birouk may be related to the effect of the specific heat of the liquid in our simulation which is variable in time and space whereas Abou Alsood and Birouk assumed a constant value for the liquid specific heat. However, our results produced better values for the evaporation rate and droplet lifetime compared with the experimental data and calculations by Abou AlSood and Birouk (2007). This can be readily observed by straight part of the d^2/d_0^2 time history curve in our results and those of Abou AlSood and Birouk (2007). The verifications of the numerical procedures and the mathematical model were examined by calculation of an evaporating droplet in a steady main flow and the flow characteristics over a non-evaporating sphere. These verifications were satisfactory to confirm the validity of the numerical code and mathematical model for investigating droplet evaporation in an oscillatory flow. In the remainder of this paper, we discuss the evaporation of a droplet in oscillatory flow.

4.2. Evaporating droplet in oscillatory flow

4.2.1. The response of evaporation to the frequency of oscillation

To determine the effect of the frequency of oscillatory flow on droplet evaporation, calculation of the flow at several frequencies was performed. In all cases, the ambiance was at 0.5 MPa and 749 K, and two oscillation Reynolds numbers, $Re_a = 15$ and 60, were considered. Fig. 5a and b shows the calculated time history of the square of droplet diameter at $Re_a = 15$ and $Re_a = 60$ at various frequencies. In the all cases the droplet evaporation rate, i.e, the gradient of d^2/d_0^2 for t/d_0^2, in oscillatory flow increases significantly compared to that in quiescent air. According to Fig. 5a for a small oscillation amplitude of $Re_a = 15$ at the low frequency of 5 Hz, the evaporation rate is maximum; however, with increasing frequency of oscillation, the droplet lifetime increases, indicating a lower evaporation rate at higher frequencies. The behavior at higher oscillation amplitude is different. At $Re_a = 60$, the increase of the flow frequency up to 15 Hz does not change the lifetime, but at frequencies higher than 15 Hz, the lifetime depends on the frequency as shown in Fig. 5b. This feature of the response of the d^2/d_0^2 time history to the oscillatory flow implies that at the higher $Re_a = 60$, the droplet responds to the flow oscillation in two different modes, depending on the oscillation frequency. The rate of heat and mass transfer from the droplet can be discussed based on the response of Nusselt and Sherwood numbers to the flow oscillation. The local Nusselt number Nu_θ and local Sherwood number Sh_θ are written as

$$Nu_\theta = \frac{2R}{(T_\infty - T_s)} \left.\frac{\partial T}{\partial n}\right|_{r=R}, \tag{19}$$

$$Sh_\theta = \frac{2R}{(Y_{f\infty} - Y_{fs})} \left.\frac{\partial Y_f}{\partial n}\right|_{r=R}, \tag{20}$$

The space-averaged Nusselt number is then defined as

$$Nu_{av} = \frac{1}{\pi}\int_0^\pi Nu_\theta d\theta, \tag{21}$$

and the space-averaged Sherwood number is

$$Sh_{av} = \frac{1}{\pi}\int_0^\pi Sh_\theta d\theta. \tag{22}$$

The trend of mass transfer is very similar to the heat transfer. Thus, in this paper, we show only the graphs of the Nusselt number. The same feature was observed for the Sherwood number. Fig. 6a and b

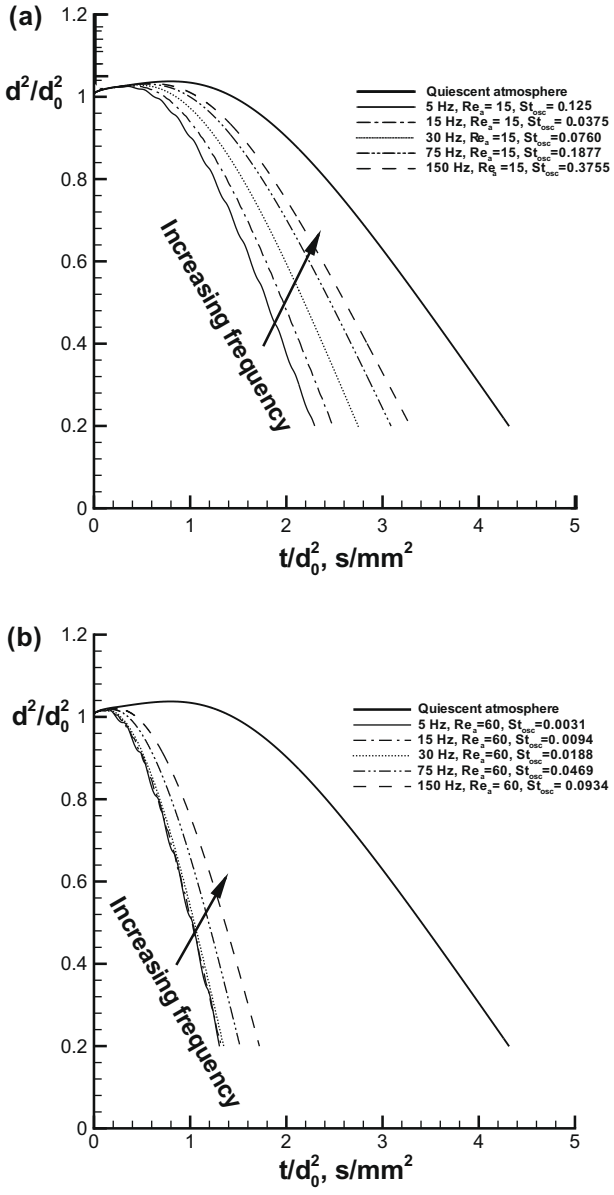

Fig. 5. Effects of the oscillation frequency on the time history of the square of the droplet diameter at ambient pressure 0.5 MPa and ambient temperature 749 K: (a) $Re_a = 15$; (b) $Re_a = 60$.

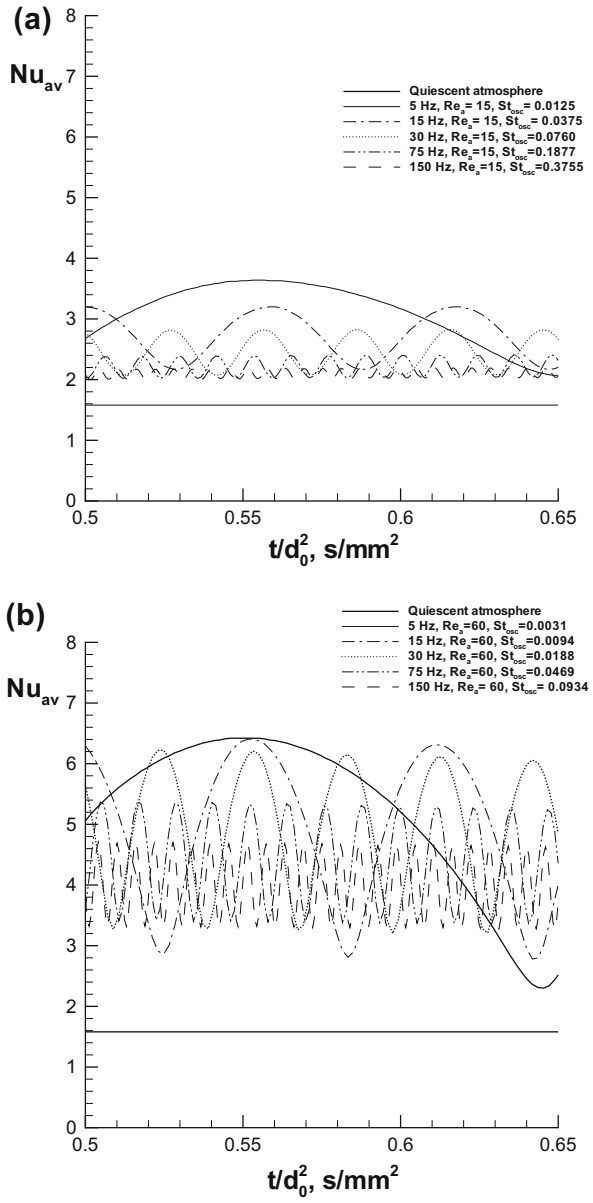

Fig. 6. Effects of the oscillation frequency on the Nu_{av} at ambient pressure 0.5 MPa and ambient temperature 749 K: (a) $Re_a = 15$; (b) $Re_a = 60$.

shows the space-averaged Nusselt number Nu_{av} in a quiescent atmosphere and oscillatory flow at $Re_a = 15$ and 60 and at various frequencies. Since the droplet was introduced to the main flow at $t = 0$ in the numerical simulation, the thickness of the boundary layer at the beginning is very thin and consequently the Nu_{av} is quite large. With development of the flow field around the droplet, the Nu_{av} decreases rapidly, and after the establishment of the boundary layer, the graph of Nu_{av} variation tends to be horizontal. It has already been shown in Fig. 5a and b that the lifetime of the droplet in oscillatory flow is less than that in quiescent air; therefore, a higher rate of heat transfer and a, respectively, larger value of Nu_{av} are expected in oscillatory flow. Fig. 6a and b clearly shown this. As was mentioned before, two modes of the time history of the square of droplet diameter were observed at $Re_a = 60$; therefore, two modes of the response of Nu_{av} at $Re_a = 60$ are anticipated. At $Re_a = 60$ and up to a frequency 15 Hz, the maximum and minimum values of Nu_{av} are the same, while for frequencies higher than 15 Hz, the response of Nu_{av} returns to what it was at $Re_a = 15$. At $Re_a = 60$ and at frequencies higher than 15 Hz, the minimum of Nu_{av} remains equal, and by increasing the frequency, its maximum decreases. It is presumed that the two modes in the time history of d^2/d_0^2 are related to these differences in Nu_{av} variation, depending on Re_a.

4.2.2. The response of evaporation to the amplitude of oscillation

Fig. 7a and b shows the time history of the square of droplet diameter at 15 Hz and 75 Hz for five Re_a. As is expected, by increasing the amplitude of oscillation the evaporation rate increases, leading to a decrease of droplet lifetime. According to our results at a frequency of 15 Hz and $Re_a = 2.5$, 15, 25, 37.5, 60, 80 the lifetime decreases 7%, 42.5%, 54%, 61%, 69% and 73%, respectively, compared to that in quicsent air. The decrease of droplet lifetime at a high frequency of 75 Hz is 5%, 28.5%, 42%, 53%, 64.5% and 70.5%, respectively. Fig. 8 shows the Nu_{av} time history at 15 Hz and 75 Hz, respectively. At 15 Hz, shown in Fig. 8a, the increase

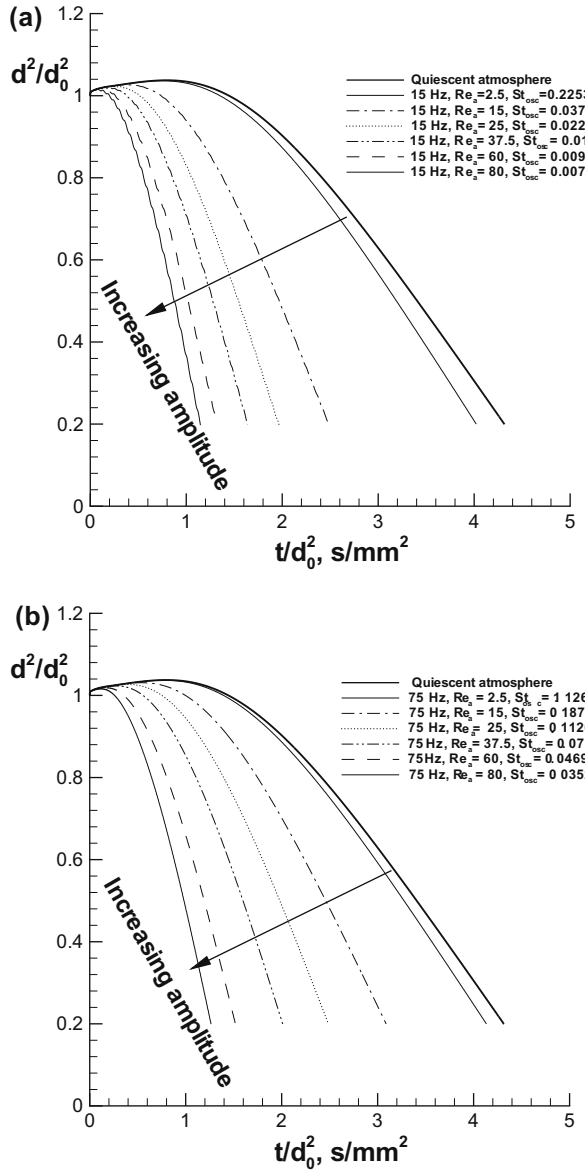

Fig. 7. Effects of the oscillation amplitude on the time history of square of droplet diameter at ambient pressure 0.5 MPa and ambient temperature 749 K: (a) $f = 15$ Hz; (b) $f = 75$ Hz.

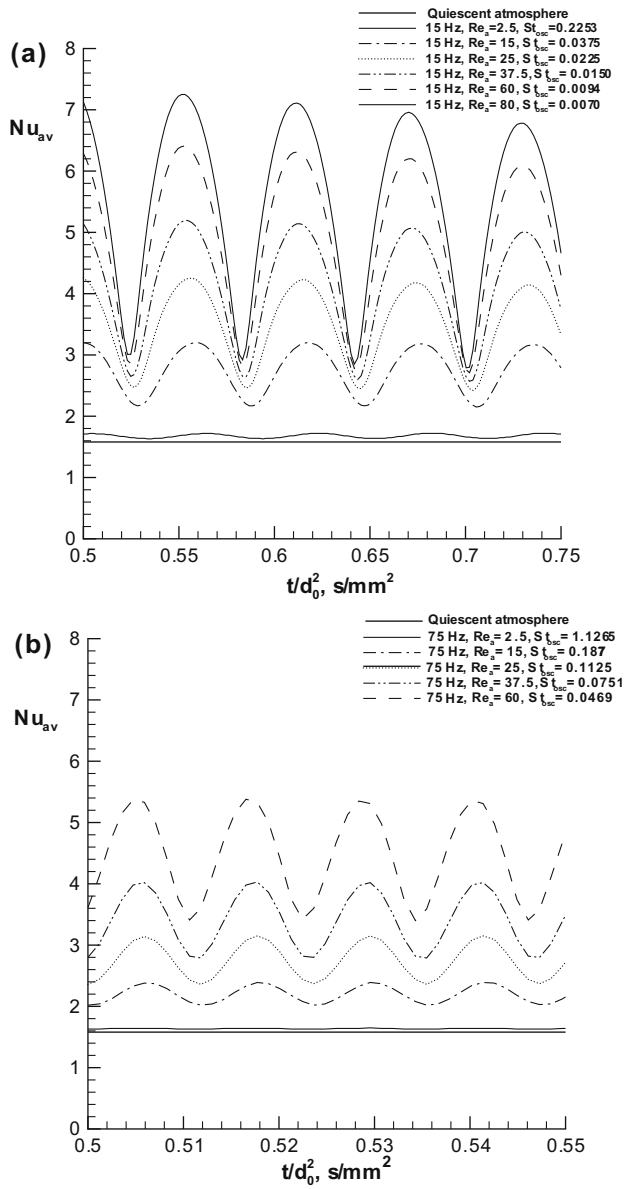

Fig. 8. Effects of the oscillation amplitude on the Nu_{av} at ambient pressure 0.5 MPa and ambient temperature 749 K: (a) $f = 15$ Hz; (b) $f = 75$ Hz.

of oscillation amplitude from $Re_a = 2.5$ to 15 results in an increase of both the minimum of Nu_{av} from 1.6 to 2.2 and its maximum from 1.78 to 3.2. This increase of the peaks occurs when the oscillation amplitude increases upto $Re_a = 60$. However, the increase of the amplitude from $Re_a = 60$ to 80 does not result in a similar behavior. In this case, by increasing the amplitude, the maximum of Nu_{av} increases while its minimum remains constant at the value the $Nu_{av} = 3$. Similar behavior as it was for 15 Hz ar $Re_a < 60$ is seen at 75 Hz, as shown in Fig. 8b. Namely, the maximum and minimum of Nu_{av} increases with increasing amplitude. In this study, other oscillation frequencies were examined, and it was confirmed that the increase of the Re_a led to an increase in the maximum Nu_{av} in all cases. The minimum Nu_{av}, however, increased first with increasing amplitude of the oscillation and then remains constant at the $Nu_{av} = 3$. Thus, it is clear that two modes of the response to the oscillation amplitude exist, which is the same phenomena as detected in the response of the evaporation process to the frequency of oscillation.

4.3. Oscillatory boundary layer around an evaporating droplet

As explained in the previous sections, there are particular features of Nu_{av} variation which depend on flow frequency and Re_a, and they may cause differences in the time history of d^2/d_0^2 variation and thus the droplet lifetime. That is, as for the frequency response, at constant amplitude, the evaporation rate is high and independent of the frequency up to a certain value. When the frequency further increases, however, the evaporation rate decreases as shown in Fig. 5b. As for the response of the amplitude, it was found that at a given frequency there is a certain Re_a above which the minimum of Nu_{av} is 3 and the maximum Nu_{av} increases due to the increase of the Re_a (Fig. 8a). However, for an oscillation amplitude less than that, both the maximum and minimum peaks of the Nu_{av} increase due to increase of oscillation amplitude. To explore the mechanism of these phenomena which affects the droplet evaporation in flow oscillation, the response of the boundary layer around the droplet was investigated. Two cases are presented here,

i.e., at the frequency of 5 Hz and $Re_a = 60$, and at the frequency of 75 Hz and $Re_a = 60$. As already mentioned, at 5 Hz the minimum Nu_{av} is almost equal to that in quiescent air (Fig. 6b). Furthermore, the evaporation rate is almost independent of the frequency change up to 15 Hz (Fig. 5b). This means that the phenomena are in a quasi-steady condition. Contrary to the case of 5 Hz, the evaporation rate is sensitive to the variation of the frequency at 75 Hz, as shown in Fig. 5b, and the minimum Nu_{av} is much larger than that in quiescent air (Fig. 6b), meaning that the phenomena in this condition are highly unsteady. Figs. 9 and 10 show three instances of the velocity vectors and temperature contours at 5 Hz and 75 Hz, respectively. At 5 Hz, when the main flow is from the right to left (Fig. 10a), the downstream heat transfer is controlled by the vortex flow while the main flow dominates upstream. At this moment, very dense temperature contours upstream clearly implies a much larger gradient of the temperature at the boundary layer upstream, meaning that a strong contribution of the heat transfer exist upstream (Fig. 9d). It can be seen in Fig. 9b, c, e and f at 5 Hz that the pattern of the boundary layer clearly follows the oscillation of the main flow, which means that the phenomena are in quasi-steady condition. For example, when the main flow velocity becomes zero, the value of the velocity adjacent to the droplet at all degrees has a very small value. Furthermore, the temperature contours as symmetrical as those in quiescent air (Fig. 9b and e). When the direction of the velocity changes, the boundary layer responds just as it does in the first half period (Fig. 9c and f). However, the behavior at the high frequency of 75 Hz is different. Fig. 10a shows velocity vectors at the moment that flow is from the right to the left. The scale of velocity vectors in Fig. 9 is equal to that in Fig. 10. Fig. 10b and e are at the moment that the main flow velocity becomes zero. As significant differences in the velocity vectors and temperature contours from those at 5 Hz (Fig. 9b and e) are seen. Dense temperature contours exist on the left-hand side due to the residual vortex motion there. Fig. 11a and b shows the variation of local

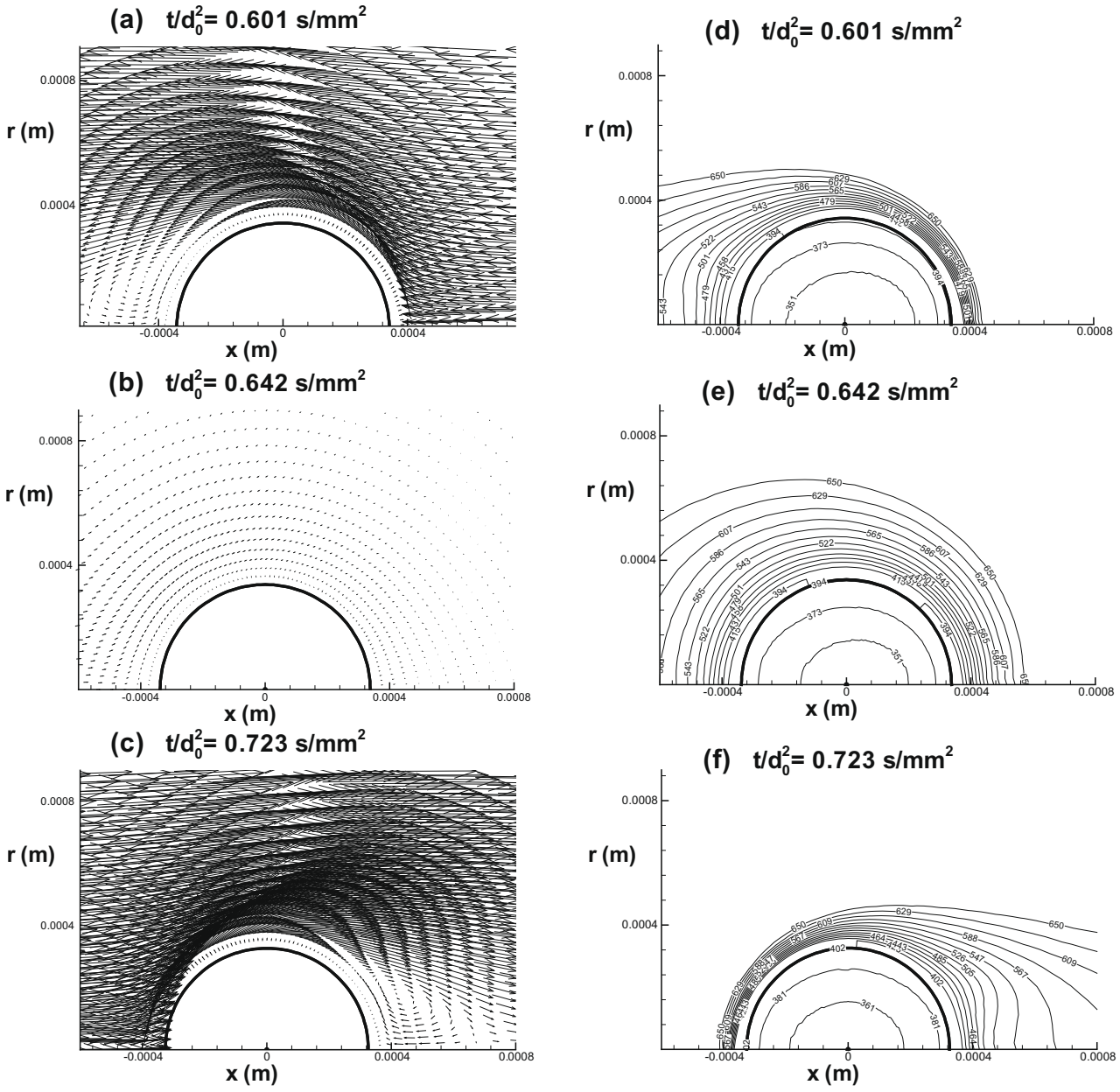

Fig. 9. Velocity vectors and temperature contours at $Re_a = 60$, $f = 5$ Hz, ambient pressure 0.5 MPa and ambient temperature 749 K; (a–c) velocity vectors in gas phase and streamtraces in liquid phase; (d–f) temperature contours.

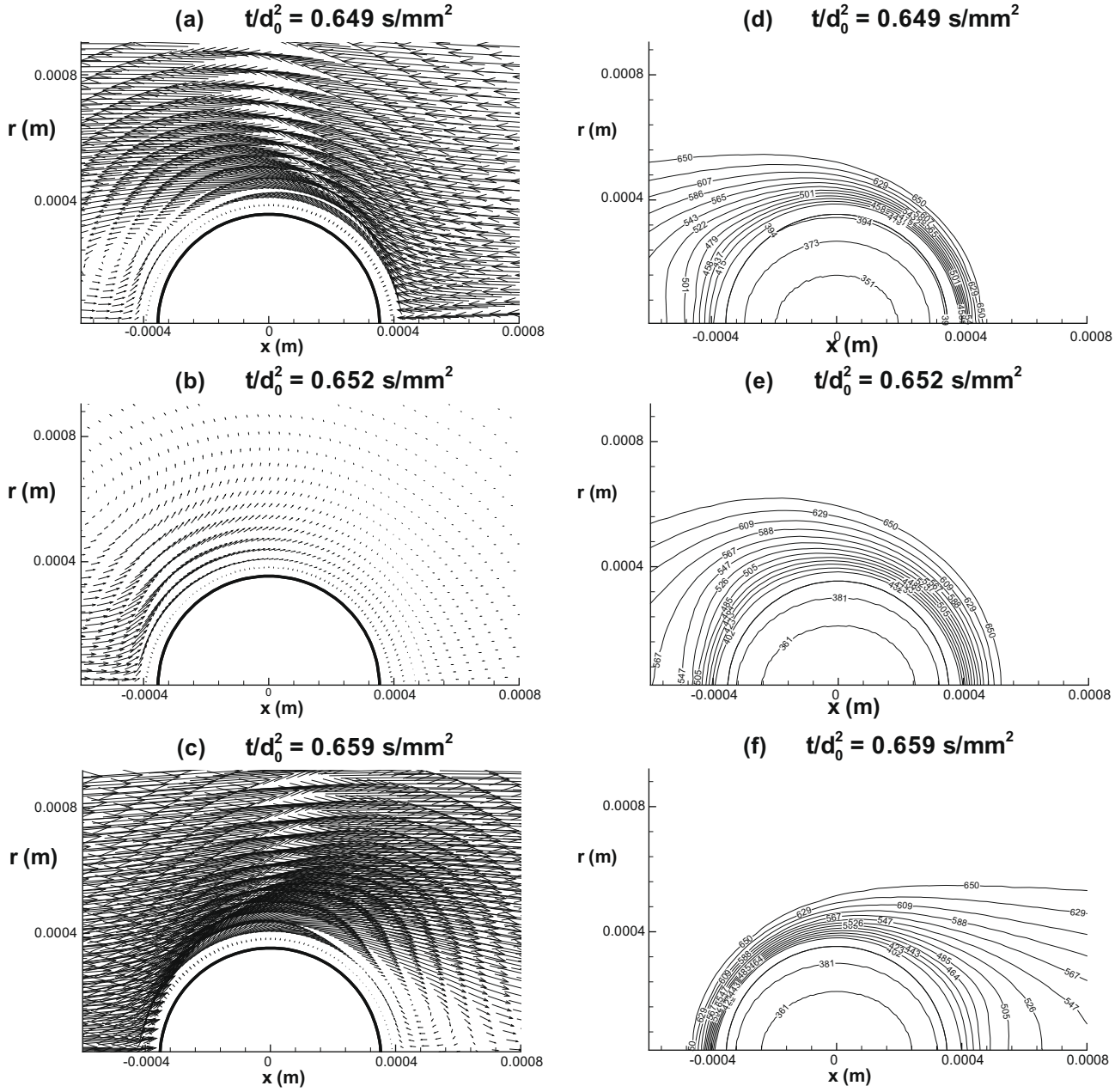

Fig. 10. Velocity vectors and temperature contours at $Re_a = 60$, $f = 75$ Hz, ambient pressure 0.5 MPa and ambient temperature 749 K; (a–c) velocity vectors in gas phase and streamtraces in liquid phase; (d–f) temperature contours.

Nusselt number Nu_θ with time at 5 Hz and 75 Hz, respectively. The synchronizing response of the boundary layer to the flow oscillation at 5 Hz clearly apparent (Fig. 11a). From this figure, we can see that with increasing velocity, the thickness of the boundary layer upstream decreases and Nu_θ increases. Decreasing velocity led to a simultaneously decrease of the Nu_θ at all degrees. For example, at the zero main flow velocity, (i.e. $t/d_0^2 = 0.642$ s/mm^2), Nu_θ at all degrees is almost equal to $Nu_{a\nu} = 2.2$. Contrary to the case of 5 Hz, the variation of Nu_θ at the high frequency of 75 Hz is asynchronous with the main flow oscillation. The Nu_θ at 75 Hz is shown in Fig. 11b at various moments. As can be seen in this figure, the contribution of heat transfer downstream at 75 Hz is larger than that at 5 Hz downstream, even though at 75 Hz the downstream dominates for some interval. This is the key mechanism of the different responses of the evaporation process to the flow oscillation at 5 Hz and 75 Hz, that is, a strong residual wake flow at high frequency produces an asynchronous evaporation response to the flow oscillation. One of the interesting findings in this study was that the two phenomena that acting in opposite ways cause residual vortex flow motion at 75 Hz. At high frequency, before there is sufficient time for the main flow to develop around the droplet, the direction of the flow changes and, thus, the average of the velocity upstream at high frequency is less than that at low frequency. The larger velocity upstream at the lower frequency of 5 Hz produces dense temperature contours upstream of the droplet (Fig. 9d) compared to the situation at 75 Hz (Fig. 10d). The higher convection rate upstream of the droplet at 5 Hz can also be seen in the Nu_θ in Fig. 11a and b, as well. The lesser rate of heat transfer means a lower evaporation rate. Therefore, the blowing velocity of evaporated fuel at 75 Hz generated by Stefan flow must be smaller than that at 5 Hz. This reduction of the blowing mass to the boundary layer itself provokes another phenome-

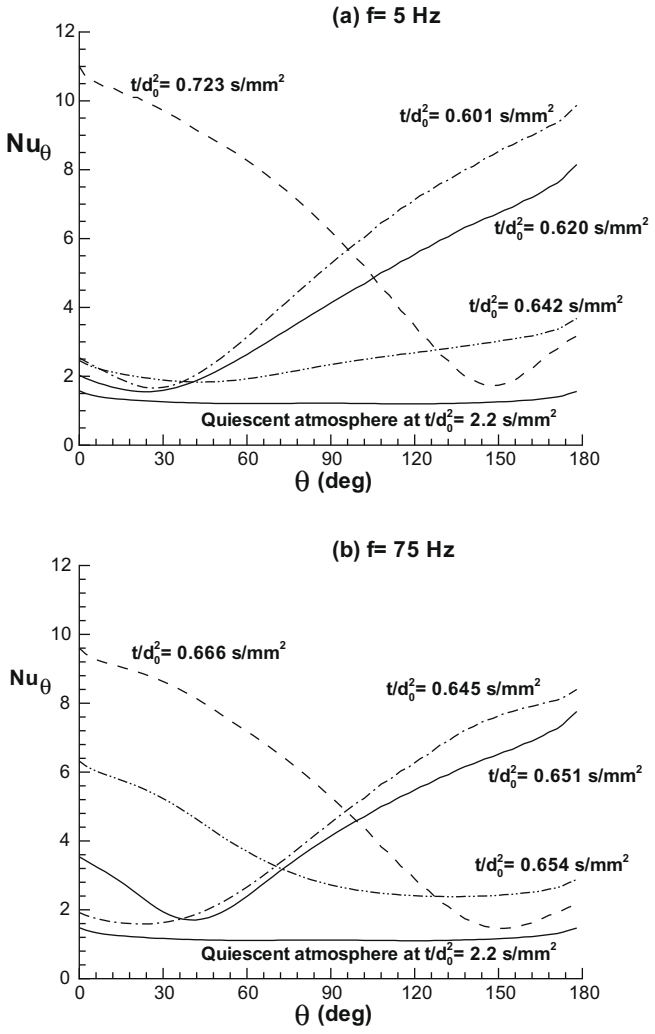

Fig. 11. Nu_θ at $Re_a = 60$, ambient pressure 0.5 MPa and ambient temperature 749 K: (a) $f = 5$ Hz; (b) $f = 75$ Hz.

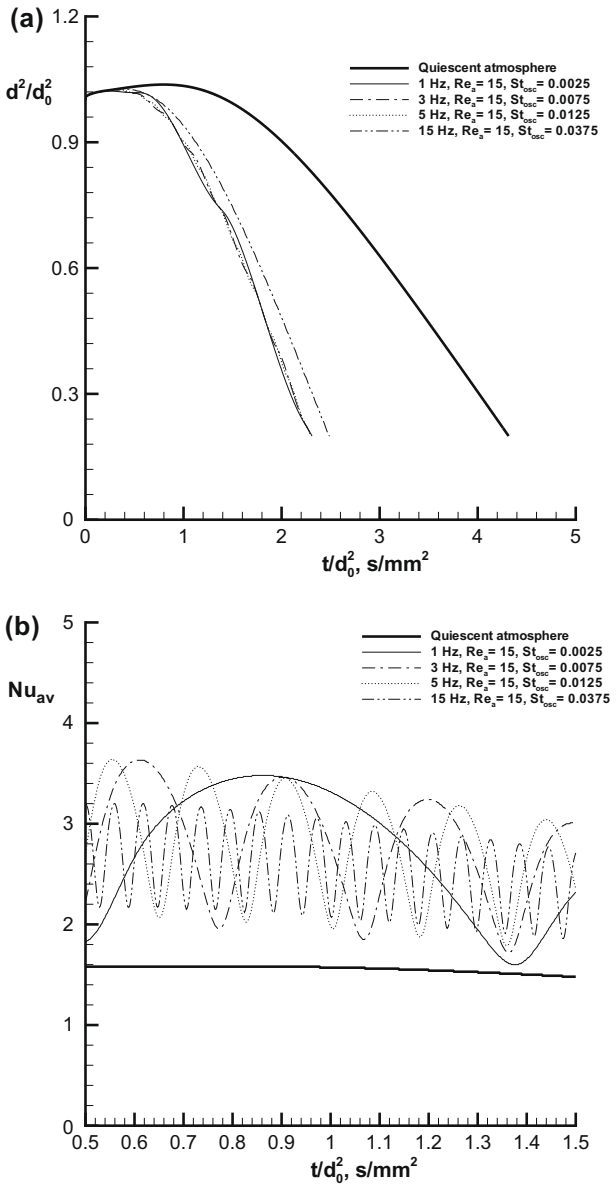

Fig. 12. Effect of S_{osc} on the response of the square of the droplet diameter and Nu_{av} at ambient pressure 0.5 MPa and ambient temperature 749 K.

non which acts in the opposite way. It is well known that blowing mass to the boundary layer causes a delay of boundary layer separation and weakens vortex motion in the wake flow. At a high frequency of 75 Hz, the blowing mass to the boundary layer is weaker. Therefore, the separation occurs at a larger angle from the forefront compared with that at 5 Hz. The larger separation region at 75 Hz means a stronger vortex motion in the wake flow, which can be clearly seen by comparison of Fig. 9a with 10a. Such a stronger wake flow generates a larger Nu_θ at 75 Hz (Fig. 11b) downstream compared with that at 5 Hz (Fig. 11a). The large, strong vortex in the wake region at 75 Hz is at especially high pressure. Therefore, as seen in Fig. 10b, the vortex motion remains even at the moment that the main flow velocity is zero, whereas at 5 Hz, the vortex has vanished (Fig. 9b). The effect of the residual wake flow can also be seen in the temperature contours (Fig. 9b and 10b). The existence of a strong, long lifetime vortex near the droplet at 75 Hz leads to enhancement of the rate of heat transfer. The interaction between the main flow variation and evaporating boundary layer in the second half period is repeated with the same features as in the first half period. Comparison between the two cases at 5 Hz and 75 Hz elucidated that the response of heat transfer in forefront and in the wake flow act in opposite ways. At high frequency, heat transfer and thus evaporation rate decrease due to the lack of the time for development of the flow around the droplet. Simultaneously, downstream enhancement of the heat transfer occurs due to the enhancement of vortex motion in the wake region and the evaporation rate is increased. It is reasonable to summarize these phenomena by defining the oscillation Strouhal number. The convection time scale of the boundary layer is

$$t_{cov} = \frac{d}{U_a} \tag{23}$$

and then the oscillation Strouhal number can be defined as

$$S_{osc} = \frac{t_{cov}}{t_{main}} = \frac{fd}{U_a}. \tag{24}$$

S_{osc} determines whether the main flow time scale is sufficiently long for development of the boundary layer over the droplet or not. Therefore, for a small S_{osc}, the quasi-steady condition is expected to be attained. As is shown in Fig. 5b, at $Re_a = 60$ and a frequency smaller than 15 Hz, the evaporation rate is independent of the oscillation frequency. Considering S_{osc} defined by Eq. (24) and using

values of $d_0 = 0.751$ mm, $f = 15$ Hz and $U_a = 1$ m/s, which are, respectively, the values of initial droplet diameter, oscillation frequency and velocity amplitude used for simulation at $Re_a = 60$ and frequency 15 Hz, the evaporation rate is expected to be independent of the frequency variation for $S_{osc} < 0.01$. Under such conditions, at $Re_a = 15$ and a frequency less than 3.75 Hz, the evaporation is not sensitive to the frequency variation. Fig. 12a shows the time history of the square of the droplet diameter at $Re_a = 15$ with frequencies no more than 15 Hz. The response of Nu_{av} at $Re_a = 15$ is shown in Fig. 12b. As is shown in these figures, The evaporation rate at $Re_a = 15$ for a frequency less than 3.75 Hz is independent of frequency, and furthermore, the minimum Nu_{av} at $Re_a = 15$ for frequencies less than 3.75 Hz meets the quiescent air line. These features of the evaporation process are very similar to those for the case of $Re_a = 60$ for frequencies less than 15 Hz.

5. Conclusions

Oscillatory convective flow was performed. Excellent agreement between present numerical results and those in the literature confirmed the validity of the code. The value of the Nusselt and Sherwood numbers, the reattachment length in wake region and separation angle in the case of flow over a sphere as well as the time history of the square of the droplet diameter in the case of evaporating fuel droplet in hot airstream were the parameters considered for comparisons.

After examination of the validity of the code, the response of an evaporating droplet to the flow oscillation was investigated numerically. The numerical results showed that with increasing amplitude of oscillation, the evaporation rate increased. As for the response of the evaporation to the frequency of oscillation, it was found that the response occurred in different modes depending on the frequency and amplitude of the oscillation. One mode of response was synchronous with the main flow oscillation and was not sensitive to the changing of the oscillation frequency. The quasi-steady condition was attained contrary to what occurred in the other mode in which the response was asynchronous with the main flow oscillation and was unsteady. However, the evaporation rate at all conditions was shown to be enhanced in oscillatory flow compared with that in quiescent air. To quantify the conditions of the transition from the quasi-steady to unsteady response, use of the oscillation Strouhal number S_{osc} was proposed in this study. This number showed whether the time scale of the oscillation compared with the flow time scale was sufficiently long to let the boundary layer around the droplet reach the quasi-steady condition or not. The numerical results showed that at a low S_{osc}, a quasi-steady boundary layer was formed, whereas by increasing the S_{osc}, the quasi-steady condition could not be attained.

Acknowledgement

We acknowledge with pleasure Professor Benjamin Shaw from the University of California at Davis for his valuable discussions and comments.

Appendix A

The following expressions were used for evaluating the thermophysical properties of liquid *n*-heptane and *n*-decane droplets (Poling et al., 2000).

n-Heptane (liquid phase)

$$\rho_l = 233.644 \times 0.26^{-(1.-T/540.2)^{0.286}} \ [\mathrm{kg/m^3}],$$
$$\mu_l = 1.57 \times 10^{-5} \exp(962.1/T) \ [\mathrm{kg/ms}],$$
$$\lambda_l = 0.101 \ [\mathrm{W/mK}],$$
$$c_{pl} = 1905 - 14.491 \times 10^{-1} T + 8.993 \times 10^{-3} T^2 \ [\mathrm{J/kg\ K}].$$

n-Decane (liquid phase)

$$\rho_l = 227.564 \times 0.247^{-(1.-T/617.6)^{0.286}} \ [\mathrm{kg/m^3}],$$
$$\mu_l = 1.16 \times 10^{-5} \exp(1286.2/T) \ [\mathrm{kg/ms}],$$
$$\lambda_l = 0.129 \ [\mathrm{W/mK}],$$
$$c_{pl} = 1760.566 + 1.406 \times 10^{-1} T + 7.285 \times 10^{-3} T^2 \ [\mathrm{J/kg\ K}].$$

References

Abou AlSood, M.M., Birouk, M., 2007. A numerical study of the effect of turbulence on mass transfer from a single fuel droplet evaporating in a hot convective flow. Int. J. Thermal Sci. 46, 779–789.
Abou AlSood, M.M., Birouk, M., 2008. Droplet heat and mass transfer in a turbulent hot airstream. Int. J. Heat Mass Transfer 51, 1313–1324.
Ambrose, D., Ghiassee, N.B., 1987. Vapour pressures and critical temperatures and critical pressures of some alkanoic acids: C1 to C10. J. Chem. Thermodyn. 19, 505–519.
Bagchi, P., Ha, M.Y., Balachandar, S., 2001. Direct numerical simulation of flow and heat transfer from a sphere in a uniform cross-flow. J. Fluids Eng. Trans. ASME 123, 347–358.
Birouk, M., Gökalp, I., 2002. A new correlation for turbulent mass transfer from liquid droplets. Int. J. Heat Mass Transfer 45, 37–45.
Birouk, M., Gökalp, I., 2006. Current status of droplet evaporation in turbulent flows. Prog. Energy Combust. Sci. 32, 408–423.
Burdukov, A., Nakoryakov, V., 1965. On mass transfer in an acoustic field. J. Appl. Mech. Tech. Phys. 2, 51–55.
Clift, R., Grace, J.R., Weber, M.E., 1978. Bubbles Drops and Particles. Academic Press, New York.
Drummound, C.K., 1990. Mass transfer from a sphere in an oscillating flow with zero mean velocity Droplet combustion in standing sound waves. Comput. Mech. 6, 315–326.
Faeth, G.M., 1983. Evaporation and combustion of sprays. Prog. Energy. Combust. Sci. 9, 1–75.
Farrashkhalvat, M., Miles, J.P., 2003. Basic Structured Grid Generation. Butterworth-Heinemann, Oxford.
Frössling, N., 1938. Gerlands Beiter. Geophys. 52, 170–175.
Gökalp, I., Chauveau, C., Simon, O., Chesneau, X., 1992. Mass transfer from liquid fuel droplets in turbulent flow. Combust. Flame 89, 286–298.
Gotoh, T., Fukayama, D., Nakano, T., 2002. Velocity field statistics in homogeneous steady turbulence obtained using a high-resolution direct numerical simulation. Phys. Fluids 14, 1065–1081.
Ha, M.Y., Yavuzkurt, S., 1993. A theoretical investigation of acoustic enhancement of heat and mass transfer – I. Pure oscillating flow. Int. J. Heat Mass. Transfer 36, 2183–2192.
Hiromitsu, N., Kawaguchi, O., 1995. Influence of flow turbulence on the evaporation rate of a suspended droplet in a hot air flow. Heat Transfer – Japan Res. 24 (8), 689–700.
Jangi, M., Sakurai, S., Ogami, Y., Kobayashi, H., in press. On the validity of quasi-steady assumption on transient droplet combustion, Combust. Flame.
Johnson, T.A., Patel, V.C., 1999. Flow past a sphere up to a Reynolds number of 300. J. Fluid Mech. 378, 19–70.
Lockwood, R., 1980. Drying food wastes with pulsating combustion. In: Proceedings of the Symposium on Pulse Combustion Technology for Heating Applications. Argonne National Lab. Report ANL/EES TM-87, pp. 224-238.
Marchese, A.J., Dryer, F.L., 1997. The effect of non-luminous thermal radiation in microgravity droplet combustion. Combust. Sci. Technol. 124, 371–402.
Marthelli, R.C., Boelter, L.M.K., 1938. The effect of vibration on heat transfer by free convection from a horizontal cylinder. In: Proc. Fifth Int. Congress of Applied Mechanics, pp. 578–584.
Masahiro, S., Masahiro, H., Masayuki, S., 1996. Enhancement of evaporation–combustion rate coefficient of a single fuel droplet by acoustic oscillation. Fuel 75, 669–674.
Masoudi, M., Sirignano, W.A., 2000. Collision of a vortex with a vaporizing droplet. Int. J. Multiphase Flow 26, 1925–1949.
Megaridis, C.M., 1993. Comparison between experimental measurements and numerical predictions of internal temperature distributions of a droplet vaporizing under high-temperature convective conditions. Combust. Flame 93, 287–302.
Mitsuya, M., Hanai, H., Sakurai, S., Ogami, Y., Kobayashi, H., 2005. Droplet combustion experiments in varying forced convection using microgravity environment. Int. J. Heat Fluid Flow 26, 914–921.
Nomura, H., Ujiie, Y., Rath, H.J., Sato, J., Kono, M., 1996. Experimental study on high pressure droplet evaporation using microgravity conditions. Proc. Combust. Inst. 26, 1267–1273.
Ogami, Y., Sakurai, S., Hasegawa, S., Jangi, M., Nakamura, H., Yoshinaga, K., Kobayashi, H., 2009. Microgravity experiments of single droplet combustion in oscillatory flow at elevated pressure. Proc. Combust. Inst. 32, 2171–2178.
Patankar, S.V., 1980. Numerical Heat Transfer and Fluid Flow, first ed. Hemisphere, Washington.

Poling, B.E., Prausnitz, J.M., O'Connell, J.P., 2000. The Properties of Gases and Liquids, fifth ed. McGraw-Hill, New York.
Riley, N., 1966. On a sphere oscillating in a viscous fluid. Quart. J. Mech. Appl. Math. 16, 461–472.
Sabnis, J.S., Lyman, F.A., 1982. Effect of oscillating flow on combustion rate of coal particles. Combust. Flame 47, 157–172.
Strahle, W.C., 1965. Periodic solutions to a convective droplet burning problem: the stagnation point. Proc. Comb. Institute 10, 1315–1325.
Tanabea, M., Kuwaharaa, T., Satohb, K., Fujimorib, T., Satob, J., Konoc, M., 2005. Droplet combustion in standing sound waves. Proc. Comb. Institute 30, 1957–1964.
Vincent, A., Meneguzzi, M., 1991. The spatial structure and statistical properties of homogeneous turbulence. J. Fluid Mech. 225, 1–20.
Vinokur, M., 1983. On one-dimensional stretching functions for finite-difference calculations. J. Comput. Phys. 50, 215–234.
Wong, S.-C., Lin, A.-C., 1992. Internal temperature distributions of droplets vaporizing in high-temperature convective flows. J. Fluid Mech. 237, 671–687.
Wu, J.-S., Lin, Y.-J., Sheen, H.-J., 2001. Effects of ambient turbulence and fuel properties on the evaporation rate of single droplets. Int. J. Heat Mass Tran. 44, 4593–4603.
Wu, J.-S., Hsu, K.-H., Kuo, P.-M., Sheen, H.-J., 2003. Evaporation model of a single hydrocarbon fuel droplet due to ambient turbulence at intermediate Reynolds numbers. Int. J. Heat Mass Tran. 46, 4741–4745.
Zhang, H., 2004. Numerical research on a vaporizing fuel droplet in a forced convective environment. Int. J. Multiphase Flow 30, 181–198.